Inner Retinal Abnormalities in X-linked Retinitis Pigmentosa with *RPGR* Mutations

Tomas S. Aleman,[1] *Artur V. Cideciyan,*[1] *Alexander Sumaroka,*[1] *Sharon B. Schwartz,*[1] *Alejandro J. Roman,*[1] *Elizabeth A. M. Windsor,*[1] *Janet D. Steinberg,*[1] *Kari Branham,*[2] *Mohammad Othman,*[2] *Anand Swaroop,*[2] *and Samuel G. Jacobson*[1]

Purpose. To investigate in vivo the retinal microstructure in X-linked retinitis pigmentosa (XLRP) caused by *RPGR* mutations as a prelude to treatment initiatives for this common form of RP.

Methods. Patients with *RPGR*-XLRP ($n = 12$; age range, 10–56 years) were studied by optical coherence tomography (OCT) in a wide region of central retina. Overall retinal thickness and outer nuclear layer (ONL) and inner retinal parameters across horizontal and vertical meridians were analyzed and compared.

Results. Retinal architecture of all patients with *RPGR* mutations was abnormal. At the fovea in younger patients, the ONL could be normal; but, at increasing eccentricities, there was a loss of photoreceptor laminar structure, even at the youngest ages studied. At later ages and advanced disease stages, the ONL was thin and reduced in extent. Inner retinal thickness, in contrast, was normal or hyperthick. Inner retinal thickening was detectable at all ages studied and was strongly associated with ONL loss.

Conclusions. Inner retinal laminar abnormalities in *RPGR*-XLRP are likely to reflect a neuronal–glial retinal remodeling response to photoreceptor loss and are detectable relatively early in the disease course. These results should be factored into emerging therapeutic strategies for this form of RP. (*Invest Ophthalmol Vis Sci.* 2007;48:4759–4765) DOI:10.1167/iovs.07-0453

X-linked retinitis pigmentosa (XLRP) is one of the severe forms of inherited retinal degeneration.[1–5] Linkage analyses showed that more than one X chromosomal locus causes XLRP,[6] and now five XLRP loci are suspected.[7] RP3, the most common molecular form, is caused by mutations in the *RPGR* (retinitis pigmentosa GTPase regulator) gene.[8] *RPGR* encodes two major isoforms. The ORF15-containing isoform of RPGR is localized to cilia in photoreceptors and other postmitotic cells and to centrosomes in dividing cells.[9–11] Interaction with other centrosomal basal body or axonemal proteins implicated in abnormal microtubular transport makes RPGR a partner in a complex set of pathways implicated in many syndromic and nonsyndromic retinal degenerative diseases.[7,11–13]

Preclinical progress has prompted thoughts of translational research leading to clinical trials in *RPGR*-XLRP.[14] Canine and mouse models are available,[9,15–17] and evidence in transgenic mice points to the possible value of gene replacement.[18] A potential problem for therapy in *RPGR*-XLRP was recently identified in the canine XLRPA2 model. Retinal remodeling was detected in these dogs whether untreated[19] or treated with intravitreal neurotrophic factor.[20] Neuronal–glial remodeling of the retina in response to photoreceptor injury has been documented in many rodent models of retinal degeneration,[21–23] in human postmortem retinal tissue from some forms of RP,[24] and most recently in humans, by means of in vivo high-resolution optical microscopy in choroideremia and Leber congenital amaurosis.[25–27] The retinal laminar architecture in human *RPGR*-XLRP, however, has not been studied in detail. We used in vivo retinal microscopy to analyze a cohort of patients with *RPGR*-XLRP as a first step toward understanding the factors that may determine feasibility and efficacy in future clinical trials of treatment for this form of RP.

Materials and Methods

Human Subjects

There were 12 patients with *RPGR* mutations, representing 11 families (Table 1). Molecular methods have been reported.[29,30] Patients underwent a complete eye examination including Goldmann kinetic visual fields, dark-adapted chromatic static threshold perimetry, and electroretinography (ERG). Techniques, methods of data analysis, and normal results have been described.[31–34] Normal subjects were included for optical coherence tomography ($n = 28$; age range, 5–58 years). Informed consent was obtained from all subjects. Procedures adhered to the Declaration of Helsinki and were approved by the institutional review board.

Optical Coherence Tomography

In vivo microscopy of the retinal cross-section was obtained with OCT (Carl Zeiss Meditec, Inc., Dublin, CA). The principles of the method and our recording and analysis techniques have been published.[35–37] Most data were acquired with the OCT3 (Carl Zeiss Meditec, Inc.) with a theoretical axial resolution in retinal tissue of ~8 μm; in three patients, data were acquired with the OCT1, with an axial resolution of ~10 μm. In all subjects, overlapping OCT scans of 4.5-mm length were used to cover horizontal and vertical meridians up to 9 mm eccentricity from the fovea. At least three OCTs were obtained at each retinal location. In a subset of patients, dense raster scans were performed to sample an 18 × 12-mm^2 region of the retina centered on the fovea.[25,26,36,37] A video fundus image was acquired by the commercial software and saved with each OCT scan. In addition, the fundus video visible during the complete session was recorded continuously on a video cassette recorder.

From the [1]Department of Ophthalmology, Scheie Eye Institute, University of Pennsylvania, Philadelphia, Pennsylvania; and the [2]Department of Ophthalmology and Visual Sciences and Biological Chemistry, University of Michigan Medical School, Ann Arbor, Michigan.

Supported by The Foundation Fighting Blindness, the Macula Vision Research Foundation, Hope for Vision, the Chatlos Foundation, the National Institutes of Health/National Eye Institute, the Macular Disease Foundation, the Ruth and Milton Steinbach Fund, and Alcon Research Institute.

Submitted for publication April 17, 2007; revised June 6, 2007; accepted August 10, 2007.

Disclosure: **T.S. Aleman**, None; **A.V. Cideciyan**, None; **A. Sumaroka**, None; **S. B. Schwartz**, None; **A.J. Roman**, None; **E.A.M. Windsor**, None; **J.D. Steinberg**, None; **K. Branham**, None; **M. Othman**, None; **A. Swaroop**, None; **S.G. Jacobson**, None

The publication costs of this article were defrayed in part by page charge payment. This article must therefore be marked "*advertisement*" in accordance with 18 U.S.C. §1734 solely to indicate this fact.

Corresponding author: Samuel G. Jacobson, Scheie Eye Institute, University of Pennsylvania, 51 N. 39th Street, Philadelphia, PA 19104; jacobsos@mail.med.upenn.edu.

TABLE 1. Molecular and Clinical Characteristics of the Patients with *RPGR*-XLRP

Patient	Age at Visit (y)	Mutation*	Visual Acuity (RE-LE)†	Refraction‡	Kinetic Visual Field Extent (V-4e)§	ERG Amplitude (% Normal Mean)‖	
						Rod b-Wave	Cone Flicker
P1	10	ORF15+483_484delGA	20/63-20/40	−1.00	87	25	23¶
P2	15	ORF15+652_653delAG	20/32-20/25	−1.50	32	10	5¶
P3	17	ORF15+474G>T#	20/40	+1.00	8	ND	ND
P4	21	ORF15+543_546delGGAG#	20/25	−4.75	55	ND	ND
P5	23	ORF15+652_653delAG	20/40	−1.25	38	20	24¶
P6	23	ORF15+990G>T#	20/25	−4.00	38	18	6
P7	23	ORF15+861G>T#	20/40	−4.25	11	ND	1¶
P8	31	ORF15+352_460dup109	20/63-20/40	−1.25	50	ND	4¶
P9	35	ORF15+del1192_1211delAAGAGG AGGAAGGAGAAGGG#	20/200	−7.50	19	ND	ND
P10**	48	ORF15+507G>T	HM	−0.50	15	ND	7¶
P11	50	1641_1644delACAA	20/400	−0.75††	<1	ND	ND
P12**	56	ORF15+507G>T	20/200-20/160	−6.25	<1	ND	ND

ND, not detectable; HM, hand motions.

* Nucleotide positions based on References 8 and 28.

† Best corrected visual acuity; similar in the two eyes, unless specified.

‡ Spherical equivalent; average of both eyes.

§ Average of both eyes; expressed as a percentage of normal mean; 2 SD below normal equals 90%.[32]

‖ Expressed as a percentage of normal mean amplitude (rod, 292 μV; cone flicker, 172 μV); 2 SD below normal equals 67% for rod b-wave and 60% for cone flicker.[33]

¶ Recorded 2 to 5 years (P1, P2, P5, and P7) or 12 to 19 years (P8 and P10) before OCTs.

Novel mutation.

** Patients are siblings.

†† Patient had cataract extraction and intraocular lens implants, both eyes.

Postacquisition processing of OCT data was performed with custom programs (MatLab 6.5; MathWorks, Natick, MA). Longitudinal reflectivity profiles (LRPs) making up the OCT scans were aligned by using a dynamic cross-correlation algorithm with a manual override when crossing structures (for example, intraretinal pigment) that interrupted local lateral isotropy of signals. Repeat scans were laterally aligned and averaged to increase signal-to noise-ratio and allow better definition of retinal laminae.[36]

Overall retinal thickness was defined as the distance between the signal transition at the vitreoretinal interface (labeled T1 in Ref. 35) and the major signal peak corresponding to the RPE.[25] In normal subjects, the RPE peak was assumed to be the last peak within the two- or three-peak scattering signal complex (labeled ORCC in Ref. 35) deep in the retina. In patients, the presumed RPE peak was sometimes the only signal peak deep in the retina; at other times, it was apposed by other major peaks. In the latter case, the RPE peak was specified manually by considering the properties of the backscattering signal originating from layers vitread and sclerad to it. Nuclear layers were defined as previously published.[25–27,35–37] Outer photoreceptor nuclear layer (ONL) thickness was defined as the major intraretinal signal trough delimited by the signal slope maxima. In some patients and at some retinal locations, ONL thickness was not measurable. An inner retinal thickness parameter was defined as the distance between the signal transition at the vitreoretinal interface and the slope maximum sclerad to the signal trough that corresponds to the inner nuclear layer (INL).[25–27,35–37]

For topographic analysis, the precise location and orientation of each scan relative to retinal features (blood vessels, intraretinal pigment, and optic nerve head) were determined with video images of the fundus. LRPs were allotted to regularly spaced bins in a rectangular coordinate system centered at the fovea. The waveforms in each bin were aligned and averaged. For two-dimensional maps, $0.3 \times 0.3\text{-mm}^2$ bins were used for sampling, whereas $0.15 \times 0.15\text{-mm}^2$ bins were used for analysis along the horizontal and vertical meridians. Overall retinal, ONL, and inner retinal thickness were measured as just described. Missing data were interpolated bilinearly, thicknesses were mapped to a pseudocolor scale, and the locations of blood vessels and optic nerve head were overlaid for reference.[25–27,37]

RESULTS

Clinical Characteristics of the Patients with *RPGR*-XLRP

Of the *RPGR* mutations in our cohort of patients (Table 1), five were novel. The others have been reported to be associated with RP.[5,29,30,38–42] All patients showed clinical and visual function features of RP (Table 1). Visual acuities were abnormal but more mildly affected in the first three decades of life than at older ages. The extent of the kinetic visual field was nearly full in response to a large bright target (V-4e) in patient (P)1, the youngest patient studied, but was diminished by at least 45% from the normal mean visual field extent in all other patients. Patterns of field loss included complete midperipheral scotomas with residual central and temporal peripheral islands (P2, P5–P7, and P9), incomplete midperipheral scotomas with residual field connecting central and temporal peripheral islands (P4 and P8), loss of peripheral field detection completely (P3, P11, and P12), and only a detectable temporal peripheral island (P10). Dark-adapted chromatic perimetry showed measurable, albeit reduced, rod function in central and/or far peripheral fields (P1, P2, and P5–P7), and the remainder of the patients had reduced cone-mediated detection of stimuli, mainly in the central field. Rod ERGs were measurable but reduced in b-wave amplitude (by ≥75% of normal mean amplitude) in some of the younger patients (P1, P2, P5, P6); cone ERGs were present but abnormally reduced (Table 1).

Topographical Maps of Retinal Thickness in *RPGR*-Mutant Retina

Maps across a wide expanse of central retina illustrate thickness topography for the full cross-section of retina, the ONL,

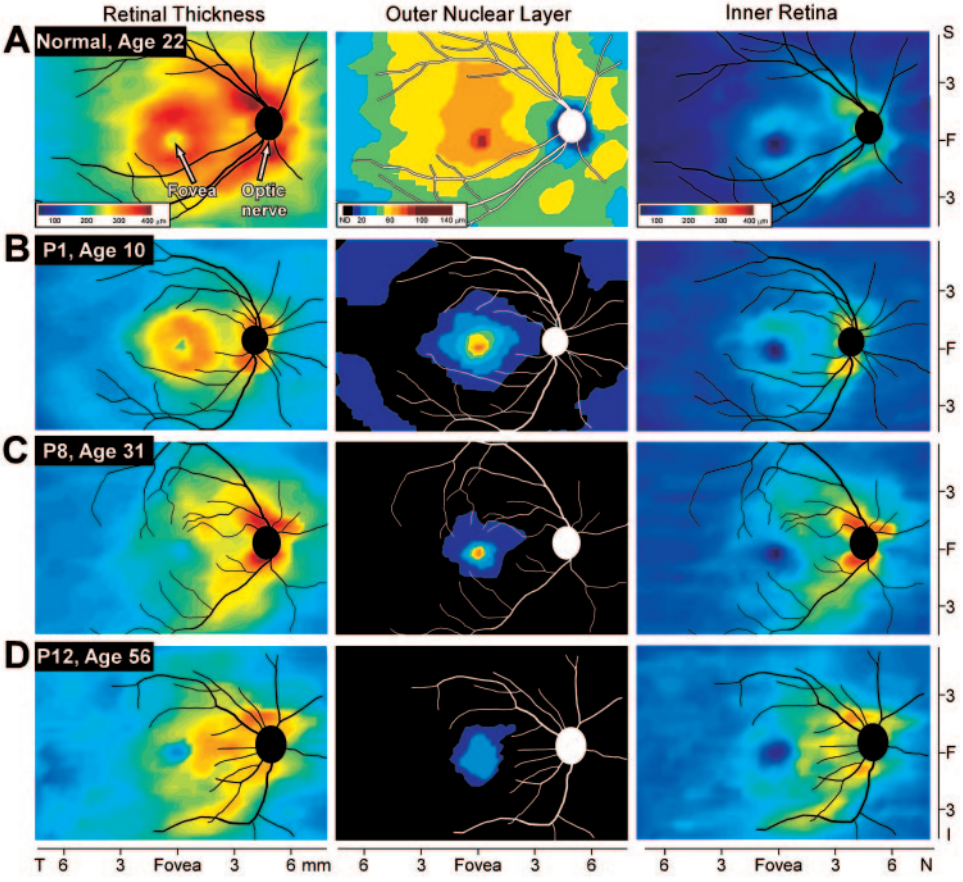

FIGURE 1. Retinal thickness topography of *RPGR*-XLRP. Topographical maps of retinal thickness (*left*), ONL thickness (*middle*), and inner retinal thickness (*right*) in a normal 22-year-old man (**A**) and three patients with *RPGR-XLRP* (P1, P8, and P12) of different ages and disease stages (**B–D**). Traces of major blood vessels and location of optic nerve head are overlaid on each map (depicted as right eyes). Note that pseudocolor scales (shown beneath the normal maps) for (**A**) and (**C**) are the same but the scale for (**B**) is different. T, temporal; N, nasal; S, superior; I, inferior.

and the inner retina in a normal subject (Fig. 1A) and three patients with *RPGR*-XLRP of different ages and disease stages (Figs. 1B–D). In the normal retina, there was a foveal depression surrounded by parafoveal thickening and then a decline in thickness with increasing eccentricity. The crescent-shaped thickening at superior and inferior poles of the optic nerve represent converging axons (Fig. 1A, left). P1, a 10-year-old patient with *RPGR*-XLRP (Fig. 1B, left), showed a similar pattern of retinal thickness to that of normal, but there appeared to be thinning across much of the central retina except at the fovea. Two older hemizygotes, P8 and P12, also showed thinned retina and thinning included the fovea (Figs. 1C, 1D, left). The ONL of the normal retina peaked centrally and declined with distance from the fovea. Parafoveal thinning occurred more gradually in the superior retina (Fig. 1A, middle). P1 retained a small central island of ONL that was surrounded by undetectable photoreceptor layer and then detectable but reduced ONL eccentric to the vascular arcades (Fig. 1B, middle). P8 and P12 also showed central ONL islands, but these were of decreased extent and thickness compared with the results in P1 (Figs. 1C, 1D, middle).

Inner retinal thickness topography in the normal retina had a foveal depression surrounded by an annulus of increased thickness and a crescent-shaped thickening extending toward the optic nerve head from the superior and inferior retina (Fig. 1A, right). Inner retinal topography in the patients with *RPGR*-XLRP approximated normal, but there were differences. There appeared to be greater thickening of the inner retina at most eccentricities from the fovea, with the older (P12) showing more thickening than the younger (P1) subject (Figs. 1B–D, right). The observations in these maps prompted us to perform locus-by-locus quantitation of thickness of overall retina, ONL, and inner retina along horizontal and vertical meridians in all 12 patients with *RPGR*-XLRP and to compare the results to those in normal subjects (Fig. 2).

Inner Retinal Architecture in *RPGR*-Mutant Retinas

Cross-sectional images in a normal subject and P2, a 15-year-old with *RPGR*-XLRP, are shown (Figs. 2A, 2B). The normal retinal cross-section had a foveal depression and the surrounding retina was laminated with two prominent low-reflectivity cellular layers (ONL and INL; highlighted) and intervening hyperreflective synaptic laminae. P2 also showed a foveal depression with normal-appearing foveal ONL thickness. The ONL, however, diminished in thickness with eccentricity from the fovea and became abnormally thin. The inner retina, including the INL and the more vitread hyperreflective layer, appeared thickened at the eccentricities with reduced ONL.

Retinal thickness, ONL, and inner retinal thickness for the 12 patients with *RPGR*-XLRP are quantified across the horizontal and vertical meridians (Figs. 2C–E). Data are plotted in relation to normal limits (defined as ± 2 SD from the mean). Patients are identified by individual symbols and colors distinguish younger (10–23 years) from older (31–56 years) age groups. Retinal thickness in the younger patients was normal or abnormally reduced, whereas the older group of patients had thinner retinas at nearly all loci across the two meridians examined (Fig. 2C). Only the youngest patients had normal ONL thickness at the fovea (Fig. 2D). In contrast to the gradual decline of ONL with eccentricity in normal data, *RPGR*-XLRP ONL became abnormally thin within the central 2 to 4 mm and remained subnormal in thickness or not detectable at further eccentricities. Inner retinal thickness was normally at a minimum in the fovea. Parafoveal thickening, a feature of the

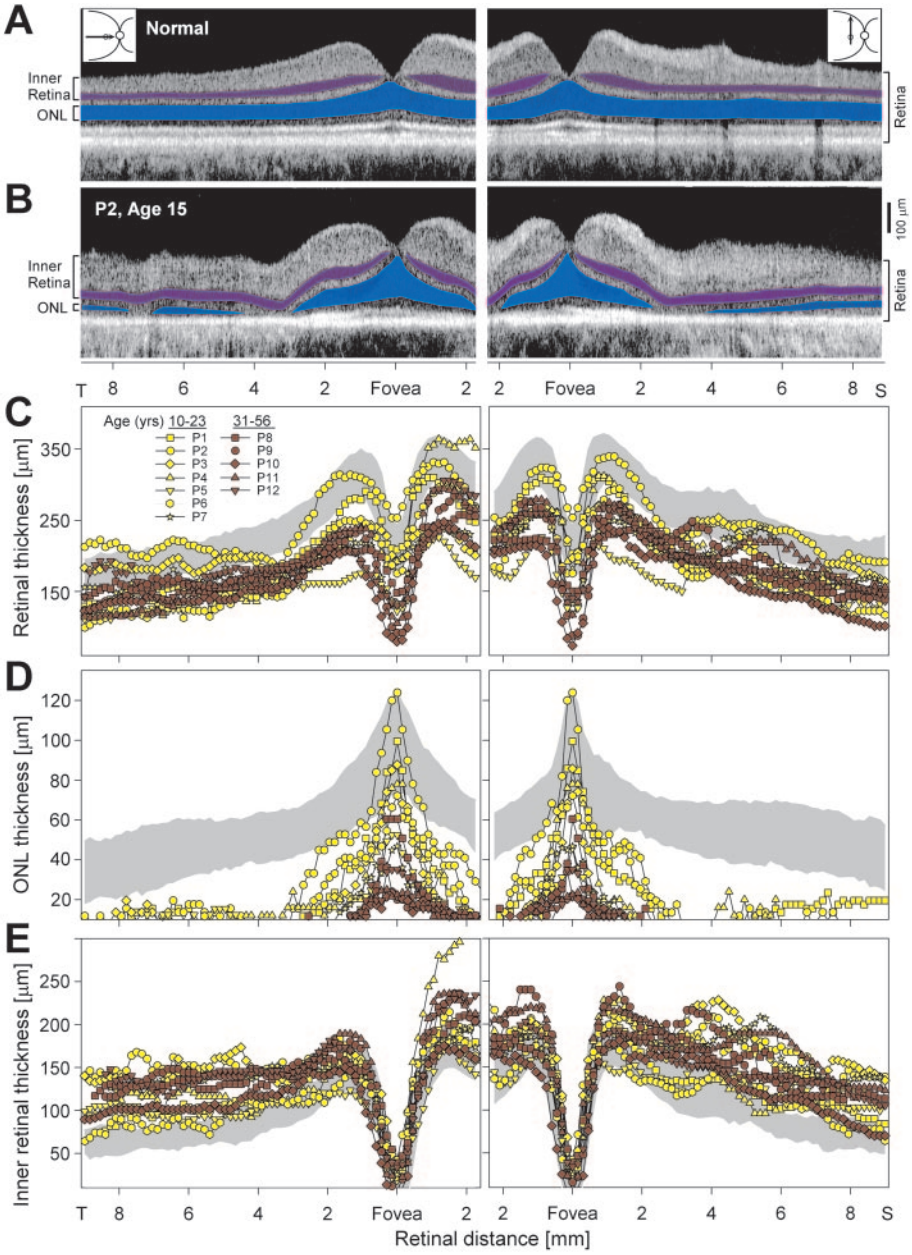

FIGURE 2. Retinal laminar architecture in *RPGR*-XLRP (**A**, **B**). Cross-sectional scans along the horizontal (*left*) and vertical (*right*) meridians in a normal subject (**A**) and a 15-year-old patient (**B**). Brackets defining ONL and inner retina are labeled (*left*) and a bracket showing total retinal thickness is at the *right*. Nuclear layers are colored (ONL, *blue*; inner nuclear layer, *purple*). OCTs are in grayscale with lowest reflectivity as *black* and highest reflectivity as *white*. *Insets*: schematic location of the scans. (**C**–**E**) Thickness of the retina (**C**), ONL (**D**), and inner retina (**E**) along the horizontal and vertical meridians in the 12 patients, identified by symbols and grouped by age. Vertical axes in (**D**) and (**E**) start at the axial resolution of the OCT system. *Shaded areas*: normal limits; mean ± 2 SD; (**C**), $n = 27$; (**D**), $n = 26$; (**E**), $n = 14$. T, temporal; S, superior.

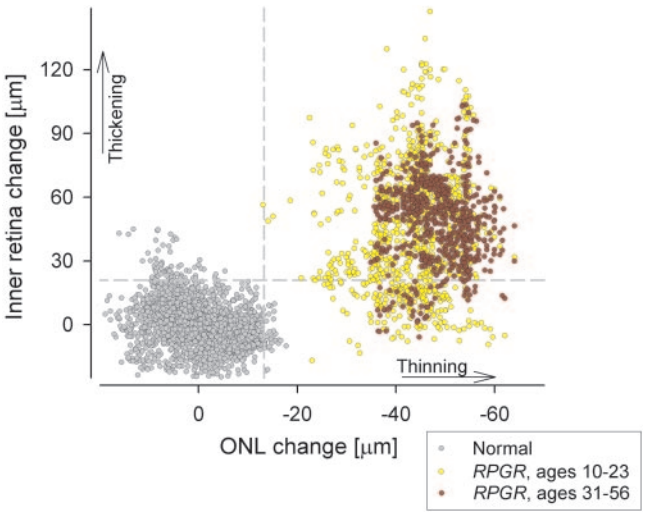

normal retina, was also present in *RPGR*-XLRP. At eccentricities beyond approximately 2 mm eccentric to the fovea, some younger patients showed normal inner retinal thickness, whereas many had hypernormal thickness. Nearly all older patients had hyperthick retinas in these paracentral regions of measurement (Fig. 2E).

We explored further the association between the primary photoreceptor loss in *RPGR*-XLRP and the observed inner

FIGURE 3. Relationship of outer and inner laminar features in *RPGR*-mutant retina. Inner retinal thickness as a function of ONL thickness at extrafoveal (>2 mm of eccentricity; 0.15 mm bins) retinal locations in patients with *RPGR*-XLRP and normal subjects. Both inner retinal and ONL thicknesses are specified as change from the mean normal value calculated at each retinal location. *Vertical dashed line*: lower normal limit (−2 SD from normal mean) for ONL thickness; *horizontal dashed line*: upper normal limit (+2 SD from normal mean) for inner retinal thickness.

retinal thickening (Fig. 3). Loci used in this analysis were outside the highly specialized foveal and parafoveal architecture[43] in the temporal, superior, and inferior retina, beginning at 2 mm eccentric from the fovea. The ONL in patients with *RPGR*-XLRP showed the expected differences from normal at these eccentricities with almost all loci (1614/1615) abnormally reduced in ONL thickness, to various degrees. The inner retina showed no loci with thinning. At the sampled loci, inner retinal thickness was either within normal limits (256/1615, 16%), or was hyperthick (84%). The younger age group had 79% (771/970) of loci with hyperthick inner retina and reduced ONL. The older age group had 91% (587/644) of loci with hyperthick inner retina and reduced ONL. In summary, the predominant finding in both younger and older patients was reduction in ONL thickness with associated thickening of the inner retina.

Discussion

Evidence that RP can be inherited as an X-linked trait dates back nearly a century (reviewed in Ref. 1). Ensuing decades have led to many studies of disease expression in XLRP hemizygotes of unknown genotype by investigators using clinical observation (for example, Refs. 4,44) and histopathology of rare donor retinas (for example, Refs. 24,45–49). The steady progress toward understanding human XLRP was accelerated by identification of causative genes and mutations (reviewed in Ref. 7). Now, there are small and large animal models of human diseases. Specifically for *RPGR*-XLRP, there are both murine and canine disease models.[9,16,17,19] This background of clinical and molecular information should help in the development of therapeutic strategies for these incurable severe blinding retinal degenerations, whether to arrest disease progression or even restore vision.

With the advent of therapeutic concepts, questions about human retinal degenerative disease have become more refined.[50] Noninvasive tools to measure retinal structure are now available to inquire whether there is treatment potential, with what possible treatment, and what age may be most appropriate.[51] In vivo microscopy by OCT permits quantitation of human retinal laminae and has been used to understand the cross-sectional micropathology of molecularly defined retinopathies.[25–27,36,37,52–55] OCT in our cohort of *RPGR*-XLRP patients revealed the expected result of retinal thinning, a well-known histopathological feature of retinal degenerative diseases in general and in XLRP in particular.[47–49] Morphometric study in XLRP donor retinas (age range, 24–84 years; mean, 62 years[47]) has reported dramatic reductions in foveal photoreceptors. Our in vivo results at the fovea showed that there can be normal ONL thickness in the first decade of life, but this becomes reduced in hemizygotes in later decades. Eccentric to the fovea, there was abnormally reduced photoreceptor laminar thickness even in the first decade of life. At late ages and more advanced stages, only a small island of central ONL remains.

Inner retinal lamination did not simply follow the ONL pattern of loss and become abnormally thin. In contrast, there was thickening of inner retinal structure. This was evident in topographical maps obtained in hemizygotes of different ages and also in most of the profiles across horizontal and vertical meridians. In general, ONL loss outside the fovea was associated with inner retinal thickening, and it was present even in the youngest ages studied. The inner retinal hyperthickness persisted into later decades. It is of interest that morphometric studies of donor retinas from patients with RP of unknown genotype (including XLRP) reported less profound cell loss in the INL than in photoreceptors or ganglion cells, both centrally and in extramacular regions, and even at late ages.[48,49]

What inner retinal abnormalities have been reported in murine or canine animal models of RPGR deficiency? A murine model of *RPGR* dysfunction, with or without an *RPGR* ORF15 transgene, showed slow but progressive ONL reduction, but inner retinal changes were not specifically mentioned.[9,17] Canine studies in XLRPA2, caused by a microdeletion in *RPGR* ORF15 with a resultant frameshift[16] have specifically studied inner retinal changes. In addition to progressive ONL thinning, the dogs had rod photoreceptor neurite sprouting that could extend deep into the inner retina, rod bipolar cell dendrite retraction, increased GABA-immunoreactive amacrine cells, and Müller glial cell reactivity that increased but later decreased. The authors concluded that such inner retinal remodeling changes occurred early rather than only late in the disease.[19] Peripheral retinal thickening and disorganization was observed in the same canine XLRP model treated with intravitreal injections of ciliary neurotrophic factor (CNTF). There was an apparent increase in the number of rod cells in the treated eyes. Also, bipolar cells had increased dendritic sprouting into the ONL. Photoreceptor nuclear phenotype abnormalities suggested dedifferentiation of rods.[20]

The exact basis of the inner retinal thickening that we observed in human *RPGR*-XLRP is not known. We speculate that the inner retinal abnormalities represent a detectable noninvasive marker for the neuronal–glial remodeling response secondary to photoreceptor stress or loss, a well-documented process in rodent models of retinal degeneration.[22,23] A clue about the basis of the *RPGR*-XLRP inner retinal abnormalities comes from similar changes noted recently in Leber congenital amaurosis (LCA) caused by *CEP290* mutations.[56] Inner retinal thickening in *CEP290*-LCA was interpreted in the context of retinal histologic abnormalities in the *rd16* mouse, a model for the human disease.[13] *Rd16* mouse retina had photoreceptor loss, but there was also inner nuclear and inner plexiform layer thickening. Surprisingly, the nuclei of the inner retinal cell types appeared enlarged; and Müller cell activation by GFAP immunolabeling was notably increased.[56] Intra- or extracellular edema may also play a role in the increased thickness of the pericentral inner retina in *RPGR*-XLRP; there was no OCT evidence of cystoid macular changes in any of the patients in the present study.

The results in our cohort of patients with *RPGR*-XLRP should be extended to larger populations of this relatively common form of RP. Focal therapeutic strategies, such as subretinal gene delivery, will require retinal structural data to determine where in the retina to deliver the treatment and what age or stage of disease is most sensible for therapy. Trials of systemically administered treatments will also gain from clear expectations of outcomes based on measurable retinal structure. An investment in understanding which patients should be included or excluded in a trial based on retinal anatomic criteria could reduce the time taken to perform a trial. Further, the exact molecular and cellular bases of the remodeling response must be elucidated in the animal models. Key unanswered questions remain, such as whether the observed inner retinal structural changes have visual functional consequences. If secondary dysfunction further complicates the primary photoreceptor disease effects and if this is not reversible, then expectations from treatment may have to be altered accordingly.

Acknowledgments

The authors thank Elaine Smilko, Mary Nguyen, Anjani Naidu, Michelle Doobrajh, Malgorzata Swider, and Waldo Herrera-Novey for critical help.

References

1. Bird AC. X-linked retinitis pigmentosa. *Br J Ophthalmol*. 1975;59: 177–199.
2. Fishman GA. Retinitis pigmentosa: visual loss. *Arch Ophthalmol*. 1978;96:1185–1188.
3. Fishman GA, Weinberg AB, McMahon TT. X-linked recessive retinitis pigmentosa: clinical characteristics of carriers. *Arch Ophthalmol*. 1986;104:1329–1335.
4. Fishman GA, Farber MD, Derlacki DJ. X-linked retinitis pigmentosa: profile of clinical findings. *Arch Ophthalmol*. 1988; 106:369–375.
5. Sandberg MA, Rosner B, Weigel-DiFranco C, Dryja TP, Berson EL. Disease course of patients with X-linked retinitis pigmentosa due to RPGR gene mutations. *Invest Ophthalmol Vis Sci*. 2007;48: 1298–1304.
6. Ott J, Bhattacharya S, Chen JD, et al. Localizing multiple X chromosome-linked retinitis pigmentosa loci using multilocus homogeneity tests. *Proc Natl Acad Sci USA*. 1990;87:701–704.
7. Shu X, Black GC, Rice JM, et al. RPGR mutation analysis and disease: an update. *Hum Mutat*. 2006;28:322–328.
8. Meindl A, Dry K, Herrmann K, et al. A gene (RPGR) with homology to the RCC1 guanine nucleotide exchange factor is mutated in X-linked retinitis pigmentosa (RP3). *Nat Genet*. 1996;13:35–42.
9. Hong DH, Pawlyk BS, Shang J, et al. A retinitis pigmentosa GTPase regulator (RPGR)-deficient mouse model for X-linked retinitis pigmentosa (RP3). *Proc Natl Acad Sci USA*. 2000;97:3649–3654.
10. Shu X, Fry AM, Tulloch B, et al. RPGR ORF15 isoform co-localizes with RPGRIP1 at centrioles and basal bodies and interacts with nucleophosmin. *Hum Mol Genet*. 2005;14:1183–1197.
11. Khanna H, Hurd TW, Lillo C, et al. RPGR-ORF15, which is mutated in retinitis pigmentosa, associates with SMC1, SMC3, and microtubule transport proteins. *J Biol Chem*. 2005;280: 33580–33587.
12. Iannaccone A, Wang X, Jablonski MM, et al. Increasing evidence for syndromic phenotypes associated with RPGR mutations. *Am J Ophthalmol*. 2004;137:785–786.
13. Chang B, Khanna H, Hawes N, et al. In-frame deletion in a novel centrosomal/ciliary protein CEP290/NPHP6 perturbs its interaction with RPGR and results in early-onset retinal degeneration in the rd16 mouse. *Hum Mol Genet*. 2006;15:1847–1857.
14. Wright AF, Shu X. Focus on molecules: RPGR. *Exp Eye Res.* 2007;85:1–2.
15. Zeiss CJ, Acland GM, Aguirre GD. Retinal pathology of canine X-linked progressive retinal atrophy, the locus homologue of RP3. *Invest Ophthalmol Vis Sci*. 1999;40:3292–3304.
16. Zhang Q, Acland GM, Wu WX, et al. Different RPGR exon ORF15 mutations in Canids provide insights into photoreceptor cell degeneration. *Hum Mol Genet*. 2002;11:993–1003.
17. Hong DH, Pawlyk BS, Adamian M, et al. Dominant, gain-of-function mutant produced by truncation of RPGR. *Invest Ophthalmol Vis Sci*. 2004;45:36–41.
18. Hong DH, Pawlyk BS, Adamian M, et al. A single, abbreviated RPGR-ORF15 variant reconstitutes RPGR function in vivo. *Invest Ophthalmol Vis Sci*. 2005;46:435–441.
19. Beltran WA, Hammond P, Acland GM, et al. A frameshift mutation in RPGR exon ORF15 causes photoreceptor degeneration and inner retina remodeling in a model of X-linked retinitis pigmentosa. *Invest Ophthalmol Vis Sci*. 2006;47:1669–1681.
20. Beltran WA, Wen R, Acland GM, et al. Intravitreal injection of ciliary neurotrophic factor (CNTF) causes peripheral remodeling and does not prevent photoreceptor loss in canine RPGR mutant retina. *Exp Eye Res*. 2007;84:753–771.
21. Jones BW, Watt CB, Frederick JM, et al. Retinal remodeling triggered by photoreceptor degenerations. *J Comp Neurol*. 2003;464: 1–16.
22. Marc RE, Jones BW, Watt CB, et al. Neural remodeling in retinal degeneration. *Prog Retin Eye Res*. 2003;22:607–655.
23. Jones BW, Marc RE. Retinal remodeling during retinal degeneration. *Exp Eye Res*. 2005;81:123–137.
24. Milam AH, Li ZY, Fariss RN. Histopathology of the human retina in retinitis pigmentosa. *Prog Retin Eye Res*. 1998;17:175–205.
25. Jacobson SG, Cideciyan AV, Sumaroka A, et al. Remodeling of the human retina in choroideremia: rab escort protein (*REP-1*) mutations. *Invest Ophthalmol Vis Sci*. 2006;47:4113–4120.
26. Jacobson SG, Cideciyan AV, Aleman TS, et al. RDH12 and RPE65, visual cycle genes causing Leber congenital amaurosis, differ in disease expression. *Invest Ophthalmol Vis Sci*. 2007; 48:332–338.
27. Jacobson SG, Cideciyan AV, Aleman TS, et al. Leber congenital amaurosis caused by an RPGRIP1 mutation shows treatment potential. *Ophthalmology*. 2007;114:895–898.
28. Vervoort R, Lennon A, Bird AC, et al. Mutational hot spot within a new RPGR exon in X-linked retinitis pigmentosa. *Nat Genet*. 2000; 25:462–466.
29. Buraczynska M, Wu W, Fujita R, et al. Spectrum of mutations in the RPGR gene that are identified in 20% of families with X-linked retinitis pigmentosa. *Am J Hum Genet*. 1997;61:1287–1292.
30. Breuer DK, Yashar BM, Filippova E, et al. A comprehensive mutation analysis of RP2 and RPGR in a North American cohort of families with X-linked retinitis pigmentosa. *Am J Hum Genet*. 2002;70:1545–1554.
31. Jacobson SG, Voigt WJ, Parel JM, et al. Automated light- and dark-adapted perimetry for evaluating retinitis pigmentosa. *Ophthalmology*. 1986;93:1604–1611.
32. Jacobson SG, Yagasaki K, Feuer WJ, et al. Interocular asymmetry of visual function in heterozygotes of X-linked retinitis pigmentosa. *Exp Eye Res*. 1989;48:679–691.
33. Aleman TS, Cideciyan AV, Volpe NJ, et al. Spinocerebellar ataxia type 7 (SCA7) shows a cone-rod dystrophy phenotype. *Exp Eye Res*. 2002;74:737–745.
34. Roman AJ, Schwartz SB, Aleman TS, et al. Quantifying rod photoreceptor-mediated vision in retinal degenerations: dark-adapted thresholds as outcome measures. *Exp Eye Res*. 2005; 80:259–272.
35. Huang Y, Cideciyan AV, Papastergiou GI, et al. Relation of optical coherence tomography to microanatomy in normal and rd chickens. *Invest Ophthalmol Vis Sci*. 1998;39:2405–2416.
36. Jacobson SG, Cideciyan AV, Aleman TS, et al. Crumbs homolog 1 (CRB1) mutations result in a thick human retina with abnormal lamination. *Hum Mol Genet.* 2003;12:1073–1078.
37. Jacobson SG, Aleman TS, Cideciyan AV, et al. Identifying photoreceptors in blind eyes caused by RPE65 mutations: prerequisite for human gene therapy success. *Proc Natl Acad Sci USA*. 2005;102: 6177–6182.
38. Sharon D, Bruns GA, McGee TL, Sandberg MA, Berson EL, Dryja TP. X-linked retinitis pigmentosa: mutation spectrum of the RPGR and RP2 genes and correlation with visual function. *Invest Ophthalmol Vis Sci*. 2000;41:2712–2721.
39. Vervoort R, Wright AF. Mutations of RPGR in X-linked retinitis pigmentosa (RP3). *Hum Mutat*. 2002;19:486–500.
40. Rozet JM, Perrault I, Gigarel N, et al. Dominant X linked retinitis pigmentosa is frequently accounted for by truncating mutations in exon ORF15 of the RPGR gene. *J Med Genet*. 2002;39:284–285.
41. Bader I, Brandau O, Achatz H, et al. X-linked retinitis pigmentosa: RPGR mutations in most families with definite X linkage and clustering of mutations in a short sequence stretch of exon ORF15. *Invest Ophthalmol Vis Sci*. 2003;44:1458–1463.
42. Sharon D, Sandberg MA, Rabe VW, et al. RP2 and RPGR mutations and clinical correlations in patients with X-linked retinitis pigmentosa. *Am J Hum Genet*. 2003;73:1131–1146.
43. Drasdo N, Millican CL, Katholi, et al. The length of Henle fibers in the human retina and a model of ganglion receptive field density in the visual field. *Vision Res.* Published online February 22, 2007.
44. Birch DG, Anderson JL, Birch EE. Early abnormalities of rod function in children with X-linked retinitis pigmentosa. *Clin Vision Sci*. 1993;8:329–335.
45. Szamier RB, Berson EL, Klein R, Meyers S. Sex-linked retinitis pigmentosa: ultrastructure of photoreceptors and pigment epithelium. *Invest Ophthalmol Vis Sci*. 1979;18:145–160.
46. Barrong SD, Chaitin MH, Fliesler SJ, Possin DE, Jacobson SG, Milam AH. Ultrastructure of connecting cilia in different forms of retinitis pigmentosa. *Arch Ophthalmol*. 1992;110:706–710.

47. Stone JL, Barlow WE, Humayun MS, de Juan E Jr, Milam AH. Morphometric analysis of macular photoreceptors and ganglion cells in retinas with retinitis pigmentosa. *Arch Ophthalmol*. 1992; 110:1634–1639.
48. Santos A, Humayun MS, de Juan E Jr, et al. Preservation of the inner retina in retinitis pigmentosa: a morphometric analysis. *Arch Ophthalmol*. 1997;115:511–515.
49. Humayun MS, Prince M, de Juan E Jr, et al. Morphometric analysis of the extramacular retina from postmortem eyes with retinitis pigmentosa. *Invest Ophthalmol Vis Sci*. 1999;40:143–148.
50. Fishman GA, Jacobson SG, Alexander KR, et al. Outcome measures and their application in clinical trials for retinal degenerative diseases. *Retina*. 2005;25:772–777.
51. Apushkin MA, Fishman GA, Alexander KR, Shahidi M. Retinal thickness and visual thresholds measured in patients with retinitis pigmentosa. *Retina*. 2007;27:349–357.
52. Jacobson SG, Sumaroka A, Aleman TS, et al. Nuclear receptor NR2E3 gene mutations distort human retinal laminar architecture and cause an unusual degeneration. *Hum Mol Genet*. 2004;13:1893–1902.
53. Cideciyan AV, Jacobson SG, Aleman TS, et al. In vivo dynamics of retinal injury and repair in the rhodopsin mutant dog model of human retinitis pigmentosa. *Proc Natl Acad Sci USA*. 2005;102: 5233–5238.
54. Schwartz SB, Aleman TS, Cideciyan AV, et al. Disease expression in Usher syndrome caused by VLGR1 gene mutation (USH2C) and comparison with USH2A phenotype. *Invest Ophthalmol Vis Sci*. 2005;46:734–743.
55. Azari AA, Aleman TS, Cideciyan AV, et al. Retinal disease expression in Bardet-Biedl syndrome-1 (BBS1) is a spectrum from maculopathy to retina-wide degeneration. *Invest Ophthalmol Vis Sci*. 2006;47:5004–5010.
56. Cideciyan AV, Aleman TS, Jacobson SG, et al. Centrosomal-ciliary gene *CEP290/NPHP6* mutations result in blindness with unexpected sparing of photoreceptors and visual brain: implications for therapy of Leber congenital amaurosis. *Hum Mutat.* Published online June 6, 2007.